Measuring the absolute decay probability of ^{82}Sr by ion implantation

C. J. Gross,[1,*] K. P. Rykaczewski,[1] D. W. Stracener,[1] M. Wolinska-Cichocka,[1,2] R. L. Varner,[1] D. Miller,[3] C. U. Jost,[1] M. Karny,[1,4] A. Korgul,[4] S. Liu,[5] and M. Madurga[3]

[1]*Physics Division, Oak Ridge National Laboratory, Oak Ridge, Tennessee 37831-6371, USA*

[2]*Oak Ridge Associated Universities, Oak Ridge, Tennessee 37831, USA*

[3]*Department of Physics and Astronomy, University of Tennessee, Knoxville, Tennessee 37996, USA*

[4]*Faculty of Physics, University of Warsaw, Warsaw PL 00-681, Poland*

[5]*UNIRIB/Oak Ridge Associated Universities, Oak Ridge, Tennessee 37831, USA*

(Received 21 December 2011; published 27 February 2012)

We have developed a method of implanted ion counting in order to determine the absolute decay probability of the 776.5 keV γ-ray transition in the decay sequence of ^{82}Sr$\rightarrow^{82}$Rb$\rightarrow^{82}$Kr. A 215 MeV beam of ^{82}Sr was produced at the Holifield Radioactive Ion Beam Facility and passed through an ionization chamber that counted and identified the ions before they were implanted into thin aluminum foils. Subsequent offline measurements using a Ge detector deduced the probability per decay of ^{82}Rb for the 776.5 keV γ ray in ^{82}Kr to be 0.1493(37), in agreement with the accepted average value of 0.1508(16). This new technique measures directly the number of decaying nuclei in a given sample and significantly reduces the dependence on knowledge of the complete decay level scheme.

DOI: 10.1103/PhysRevC.85.024319 PACS number(s): 21.10.−k, 23.20.−g, 23.40.−s, 27.50.+e

I. INTRODUCTION

The decay properties of radioisotopes should be well understood in order to use them for specific purposes. One such property is the absolute decay probability of a specific, easily observed energy transition. From this, one can determine the number of nuclei of the isotope in an unknown sample. The decay probability can be measured in a straightforward manner by knowing the number of nuclei of the isotope in a given sample and measuring the yield of the transition in a well calibrated γ-ray detection system. However, it is difficult to know the number of nuclei to sufficiently high precision. With the recent development of facilities that produce high-energy radioactive ion beams, it is possible to count each nucleus in a given sample. This paper describes this new technique for determining the ^{82}Sr-^{82}Rb-^{82}Kr decay sequence.

The radionuclide ^{82}Rb has been used for many years in positron emission tomography (PET) to image the heart muscle. In fact, a special issue [1] of the *Journal of Applied Radioation and Isotopes* was devoted to the subject and to the nuclear physics of the ^{82}Sr-^{82}Rb generator upon which it depends. Suppliers of ^{82}Sr typically use the 776.5 keV γ-ray transition in ^{82}Kr as a measure of how many ^{82}Sr nuclei are in the generator. This transition is isolated in the decay spectrum and its intensity can be easily determined with modern Ge detectors. In 1987, two groups reported the probability per decay of ^{82}Rb to emit a 776.5 keV γ ray following β decay. Their results, 0.1512(18) [2] and 0.149(4) [3], differed significantly from the previously accepted value of 0.134(5) [4] obtained using low-resolution NaI(Tl) detectors. The currently accepted value [5], 0.1508(16), is the weighted average of the two newer measurements.

The two 1987 measurements were made under similar conditions. They

(i) determined relative γ-ray emission rates by using high resolution Ge or Ge(Li) detectors;
(ii) measured positron emission rates by detecting annihilation radiation;
(iii) determined the probability of annihilation radiation and x-ray emission per decay using calculated electron-capture-to-positron ratios.

Thus, the systematic errors of both measurements are similar, and are dependent upon knowledge of a complete decay scheme for ^{82}Rb in order to correctly apply the theoretical electron-capture-to-positron ratio. We have undertaken the present study to minimize this systematic uncertainty and to measure directly the decay probability of the 776.5 keV transition. Our technique has the added benefit of removing much of the chemistry and thus significant impurities from other isotopes. In addition, it is applicable to most radioactive species including extremely short-lived isotopes, as demonstrated by the absolute β-delayed neutron probabilities reported for ^{76,77,78}Cu and ^{83}Ga fission fragments [6,7].

II. EXPERIMENTAL TECHNIQUE

Our technique is to produce a beam of ^{82}Sr and accelerate it above 2.5 MeV per nucleon at the Holifield Radioactive Ion Beam Facility (HRIBF) [8] at Oak Ridge National Laboratory. The beam is delivered to an ionization chamber that counts individual beam particles and measures their energy loss in the gas. The acceleration process selects particles by mass and thus eliminates most contaminants. The energy loss of the beam in the ionization chamber is element specific at these energies, enabling identification of the remaining contaminants. The ions are implanted into thin foils placed in the gas immediately after the last anode of the ionization chamber. These foils can

*grosscj@ornl.gov

then be removed from the chamber and the decay spectrum measured with a well-calibrated γ-ray analysis system. This technique counts every ion that gets implanted and hence the decay probability can be measured directly without relying on theoretical calculations or knowledge of the feeding to higher energy levels.[1]

A. Radioactive ion beam production

The 370 MBq ^{82}Sr sample was purchased and shipped in a vial with a few drops of weak HCl. This solution was dropped into copper powder in a copper cup, capped with additional powder, pressed, and heated in air to convert the $SrCl_2$ to SrO. The cup was then placed in the copper cathode holder of the HRIBF multisample sputter source [9] where Cs ions bombarded the powder, ejecting negative ions of SrO from the cathode. The SrO^- molecule was extracted from the source, formed into a beam, mass analyzed, and injected into the 25 MV tandem accelerator. The molecule was dissociated in the gas stripper located in the high-voltage terminal of the tandem, and $^{82}Sr^+$ was further accelerated to 215 MeV. A 90° energy-analyzing magnet selected the monoenergetic beam of ^{82}Sr that was delivered to the experimental end station.

The first test run indicated that improvements could be made. A significant problem was the purity of the beam when the powder used to hold the SrO was copper. Despite the beam analysis techniques used, the Sr beam was only 10% of the total beam delivered to the implantation station. The impurity is believed to be copper which resulted from negative ions of $^{63}Cu^{35}Cl$ that have the same mass as $^{82}Sr^{16}O$. In fact, the negative ion beam current up to the terminal of the tandem was several nanoamperes, which could only be from a stable contaminant. Even though the beam had passed through a 180° magnet and the energy-analyzing 90° magnet, a contaminant was delivered to the implantation station on the order of 13 000 ions/s, representing a reduction in beam intensity relative to the terminal of over seven orders of magnitude. The intensity and composition of the impurity was strongly affected by small energy changes, suggesting it was not ^{82}Se, the only possible ^{82}Sr isobar. In this initial attempt, the ^{82}Sr intensity was 1300–2000 ions/s and would have been adequate for our measurements if not for the high impurity of the beam.

To reduce the contamination, our next attempt used silver powder instead of copper and replaced copper cups with tantalum cups. Previous experience in developing Be beams [10] indicated that Ag should give comparable results but would significantly reduce the copper that can be sputtered. Indeed, our ^{82}Sr beam intensity remained unchanged or slightly lower (1600 ions/sec) while reducing the copper contamination by a further order of magnitude (800 ions/sec). The overall reduction in total beam intensity also benefited the ion counting. Obvious future improvements to this ion source would be to replace the copper cathode holder with a different material such as tantalum. The ion-source cathode assembly used in the second production run is shown in Fig. 1.

FIG. 1. (Color online) Photograph of the ion-source cathode assembly for the second production run. Four cathodes are filled beginning clockwise from the upper-right position: ^{nat}Sr in Ag, ^{nat}Sr in Cu, ^{82}Sr in Ag, and ^{nat}SrO in Cu. The cathodes with Ag are in Ta cups and the others are in Cu holders. The first three cathodes were produced using the same technique. The fourth was produced by mixing SrO powder with Cu powder before filling and pressing.

B. Beam counting and implantation

The ^{82}Sr beam was tuned to a focus on a red alumina phosphor a short distance upstream from the entrance window to the ionization chamber [11]. The ionization chamber is comprised of six 9 mm anodes separated by 1 mm with a common cathode of approximately 60 mm. The typical configuration [11] uses entrance and exit windows that are 16 mm in diameter with metal support wires for the 0.9 μm mylar windows. The chamber is filled with CF_4 gas and can be operated as high as 270 mbar. In the present experiment, 150 mbar was found to provide good identification of ions while ensuring the ions had enough energy to be implanted into thin kapton or aluminum foils of 19 mm diameter.

The detector signals were processed through standard analog electronics that digitized the peak height of each pulse from all anodes. The signal from the second anode provided an event signal to start the data acquisition system. The ratio of triggers counted when the data acquisition was live to the total triggers was a measure of the effective live time of the system. A pulser signal was injected onto the second anode to monitor electronic gain shifts and to provide a further check on live time. In addition, a 100 Hz clock was similarly counted and yielded a third estimate of the live time. In order to be counted as a probable implantation event, all six anodes of the ionization chamber were required to register a signal. A sketch of the ionization chamber and the relevant electronics are shown in Fig. 2.

[1]To do a full correction for γ summing, knowledge of the preceding γ transitions is needed. However, this correction and uncertainty is typically much smaller than other uncertainties.

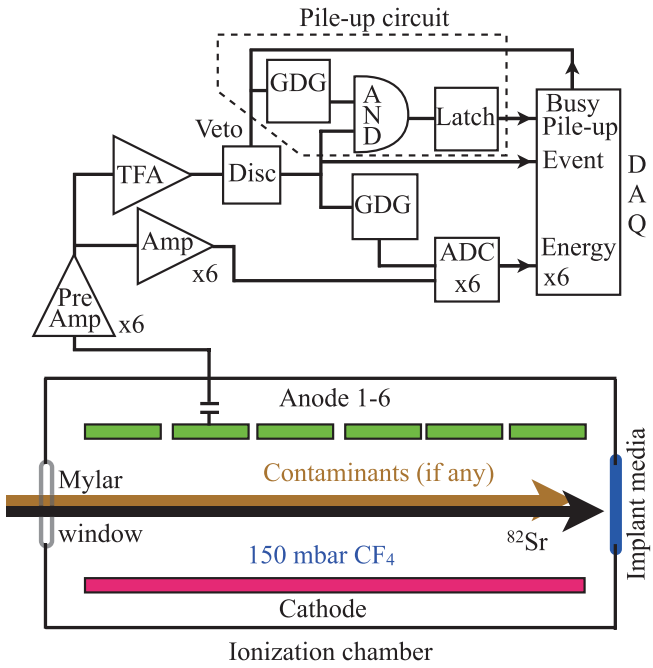

FIG. 2. (Color online) Sketch of the ionization chamber and its data acquisition (DAQ) electronics. The beam entering the mylar window should be ∼2.5 MeV/nucleon. Only the circuit for anode 2 is shown. The other anodes have the preamplifier (Pre Amp), shaping amplifier (Amp), and peak sensing analog-to-digital converter (ADC) circuit. The preamplifier signal is split between the Amp-ADC circuit and the timing filter amplifier (TFA) discriminator (Disc) circuit which initiates the event, provides the delayed gate (GDG) for the ADC, and identifies the pileup events using the busy-out from the DAQ and a gate-AND-Latch circuit. The end of the gate signal is matched to coincide with the end of the ADC gate. Scalers, not shown, were also used.

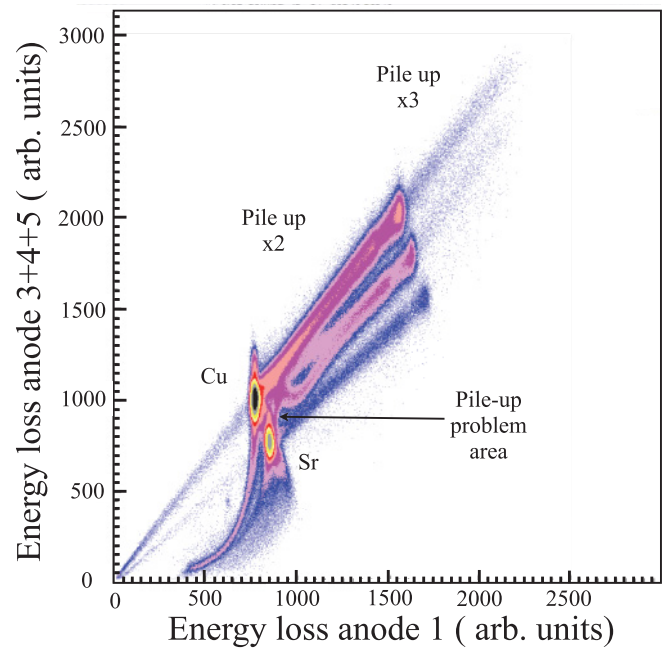

FIG. 3. (Color online) Energy loss spectrum from the test run. Labels identify the features of data and color changes represent reductions in intensity by factors of approximately 3.33, with black indicating an intensity of 60298 counts/pixel and dark blue indicating 3 counts/pixel. The pileup circuit discussed in the text was later used to identify events indicated by the arrow. See Figs. 6–8 for the improved data from the production run.

During the test run several data acquisition problems were identified. The most significant problem was the high data rate and the pileup that resulted. Pileup occurred when a second ion (or more) entered the ionization chamber during the time it took to process the signals from the first ion. If the second ion pulse occurred after the analog-to-digital converter (ADC) gate closed, it did not affect the spectrum and was accounted for in the analysis by the live-time correction. If it occurred while the ADC gate was open, the pileup signal may be only partially integrated, thus appearing in the spectra on a continuum of events with higher than normal energy loss extending up to twice (or more) the full energy of a non-pileup event. The closer together in time the ions occur, the closer to twice the full energy loss was recorded. This can be seen in the energy-loss spectrum shown in Fig. 3. Although many of the pileup events can be identified and counted, those close to the energy loss of a single ion cannot be disentangled and may result in significant (a few percent) uncertainty in the number of atoms. In addition, the high counting rate from the detector resulted in excessive dead time in the acquisition system. This dead time was reduced by scaling down by a factor of 10 the rate of events processed. The production run with its much lower total beam intensity allowed the removal of the scale-down. A faster readout controller was also added to cut the data processing time by almost half. In addition, a pileup circuit was added to identify pileup events that occur after the data acquisition inhibit was initiated.

Another problem identified was the presence of the exit window support wires. Although they represent a small fraction of the total area of the window, any ion recorded by the ionization chamber that hits the wires is lost in the implantation. Therefore, this window was removed and the foil position was moved closer to the last anode so that the resulting path did not increase the amount of gas the ions must traverse. The size of the tandem beam is typically small: on the order of 2 or 3 mm diameter or less. As it passes through the ion chamber window and gas, the processes of slowing down and multiple scattering are assumed to result in a Gaussian distribution of implanted ions centered about the beam axis. We estimate this distribution to have a full width at half-maximum of 7.5 mm or less, as determined by the lack of detectable (3σ) ^{82}Sr on the implantation foil ring holder.

A silicon detector was mounted temporarily in place of the foil and measured the implantation efficiency as better than 99.5% in our calibration runs. There were events in the ionization chamber that were missing from the silicon detector coincidence corresponding to low-energy events in all six anodes. Events falling inside two-dimensional regions or gates of the energy loss spectra—see Fig. 3—effectively contain both low- and high-energy thresholds, rendering a separate correction for implantation efficiency unnecessary under normal operating conditions.

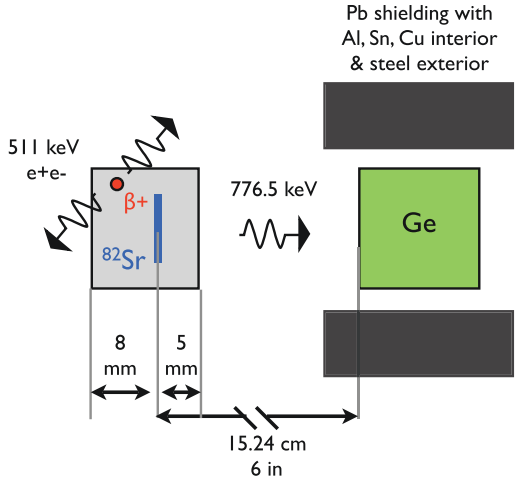

FIG. 4. (Color online) Sketch illustrating the setup for the γ-ray measurements.

C. Offline analysis

A standard n-type Ge detector with 15% intrinsic efficiency was used to measure the decay of the implanted ions. The energy resolution was better than 2 keV at 1.33 MeV and was calibrated for efficiency using several standard 3 mm diameter sources [12] mounted on thin kapton foils. These sources provided transitions from ^{241}Am, ^{109}Cd, ^{133}Ba, ^{152}Eu, ^{139}Ce, ^{57}Co, ^{85}Sr, ^{54}Mn, ^{88}Y, and ^{60}Co. This source combination had the advantage that ^{152}Eu has a 778.9 keV γ ray that is less than 3 keV from the line of interest, includes a potential contaminant ^{85}Sr, and covers the energy range from 61 keV to over 1800 keV. The γ-ray analysis station was calibrated for 15 and 30 cm geometries and with and without thick aluminum positron annihilators surrounding the sources. Ultimately, the 15 cm geometry was used with positron annihilators in place, as is shown in Fig. 4. The Ge detector was shielded by an annular cylinder with layers of steel, lead, tin, copper, and aluminum.

The absolute efficiency for 776.5 keV γ rays was fit globally (down to 61 keV) and for the higher energies (above 340 keV) using two different polynomial least-squares formalizations [13]. The center of the range of four resulting efficiencies was taken as the efficiency value with the range limits giving the uncertainty.

III. RESULTS

Following the experience in the first test run, the following parameters were chosen for the second implantation run:

(i) ^{82}Sr beam was produced using pressed silver powder cathodes in tantalum cups.
(ii) ^{82}Sr beam energy was 215 MeV.
(iii) Ionization chamber used CF_4 gas at 150 mbar.
(iv) Pileup circuit was added with fast data readout and no scale-down of the trigger rate.
(v) No exit window was on the ionization chamber.
(vi) Aluminum implantation foils were placed approximately 3 mm from the edge of the last anode.
(vii) 100 Hz pulser and event rate were used for live-time corrections.

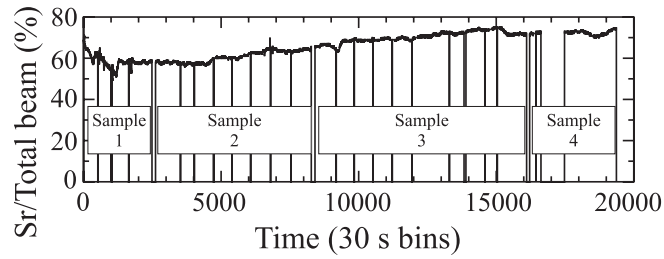

FIG. 5. Concentration profile of ^{82}Sr in the beam throughout the experiment. Data are sorted into 30 s time bins and based on gates set in the two-dimensional energy loss spectra, an example of which is shown in Fig. 6. The time region corresponding to each sample implantation is indicated on the figure.

(viii) γ-ray counting used the 15 cm geometry and aluminum annihilators.

The beam was delivered over a period of 7 days with total beam intensity ranging from 1800 to 2500 ions/s. During this time, four different foils were implanted. The data were sorted into time bins of 30 s. The profile of the ^{82}Sr component in the beam is shown in Fig. 5.

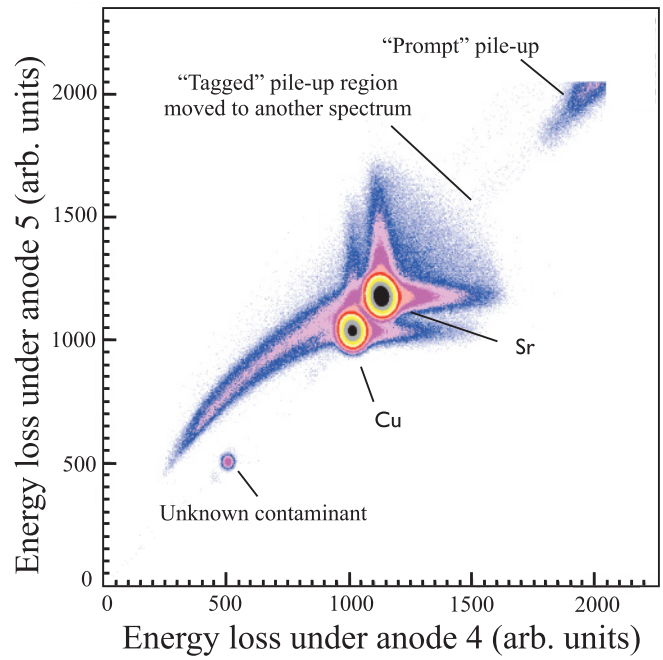

FIG. 6. (Color online) Energy loss spectrum from the production run not tagged as pileup. Pileup data exists beyond the region shown (see Fig. 8). Labels identify the features of data and color changes represent reductions in intensity by factors of approximately 3.33, with black indicating an intensity of 51391 counts/pixel and dark blue indicating 3 counts/pixel. A two-dimensional gate enclosed the events labeled Sr and Cu and included the wings to the right and above each intense group. Narrow gates, discussed in the text, did not include the wings and were drawn tightly around the circular intense regions. The pileup circuit discussed in the text resulted in the lack of data in the region indicated. The data corresponding to this region are shown in Fig. 7.

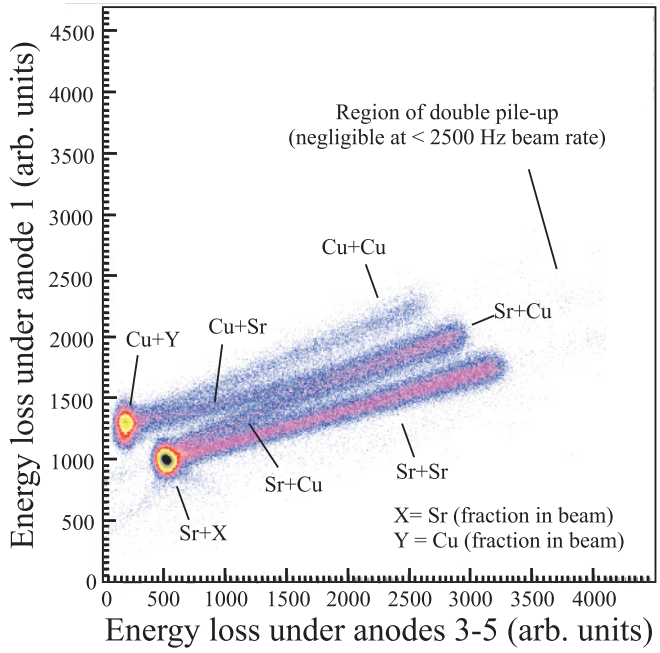

FIG. 7. (Color online) Energy loss spectrum from the production run tagged by the pileup circuit. See text concerning the full-energy single events labeled with X and Y. Labels identify the features of data and color changes represent reductions in intensity by factors of approximately 3.33, with black indicating an intensity of 148 537 counts/pixel and dark blue indicating 4 counts/pixel.

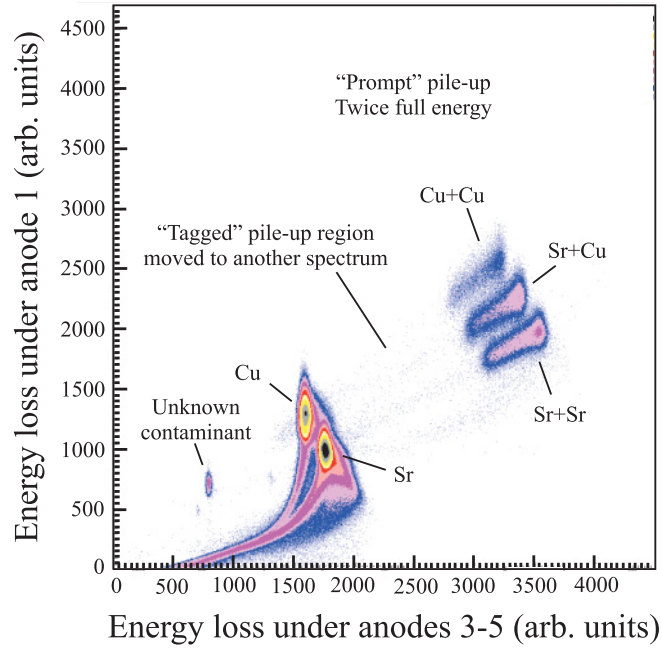

FIG. 8. (Color online) Energy-loss spectrum from the production run not tagged by the pileup circuit. The high-energy events correspond to pileup events that occurred before the pileup circuit could be initiated to detect them. Labels identify the features of data and color changes represent reductions in intensity by factors of approximately 3.33, with black indicating an intensity of 319 counts/pixel and dark blue indicating 2 counts/pixel.

An implantation event was defined to be an ion that produced a signal in all anodes. Two-dimensional gates were set on the fourth and fifth anode spectrum, which provided the best separation of the beam components as a result of the addition of the pileup identifier. A representative example of the data is shown in Fig. 6. These single-ion events accounted for approximately 97% of all events.

The remaining 3% of events were identified as pileup in either the pileup identification tag or as events of nearly twice the energy loss of single ion events. Representative examples of the spectra used to count these events are shown in Figs. 7 and 8. All events in Fig. 7 and the high-energy events in Fig. 8 represent two beam particles processed as a single event. Their location in the spectrum provides sufficient identification for each particle, with the exception of those events in the same area as the full-energy single events in Fig. 7. These events correspond to those that occur in the time near the close of the ADC gate where one event has been completely processed and identified while the other has not. The sum of these unidentified events is proportional to the beam, and hence is best approximated by the percent contribution of the beam components. Thus, in the pileup spectrum, the single full-energy ^{82}Sr events count as two ^{82}Sr ions and the single full-energy contaminant ions count as two contaminant ions.

Two methods were used to determine the number of ^{82}Sr ions implanted into the foils. One method (A) involved summing two-dimensional gates around the appropriate groups in the spectra shown in Figs. 6–8. The other method (B) determined the fraction of ^{82}Sr (see Fig. 5) in the beam as given by the ratio of the two-dimensional gates around the full-energy single event spectrum shown in Fig. 6. This fraction was then multiplied by the total number of events recorded, adjusted for pileup events (tagged and untagged). The number of untagged events was determined by the number of high energy events above the pileup tagged region as shown in Fig. 8. In addition, a low-energy threshold was used to account for the low-energy events that were not implanted, as revealed in the silicon detector implantation efficiency tests. Method B was checked using the same large gates of method A as well as extremely tight circular gates drawn around the full-energy peaks. Both methods (and the narrow-gate check) yielded the same value within less than 0.1% of each other.

The four implanted sample foils were stacked together and measured for γ emission. By correcting each 30 s time bin for the half-life of ^{82}Sr, 25.35(3) days [3,5,14], the total number of ^{82}Sr atoms remaining in the four samples at the start of the γ measurement was $7.264(27) \times 10^8$ atoms (the average of the two methods). The general size of the corrections and their uncertainties included in the number of atoms remaining includes

(i) implantation efficiency, 1.000(3) and 0.995(3), applied globally;
(ii) data acquisition live time, typically 0.910(2), adjusted per sample;
(iii) statistical error, applied on each 30 s time bin;
(iv) fractional purity (applicable to method B only), applied on each 30 s time bin;
(v) half-life of 25.35(3) d, applied on each 30 s time bin;

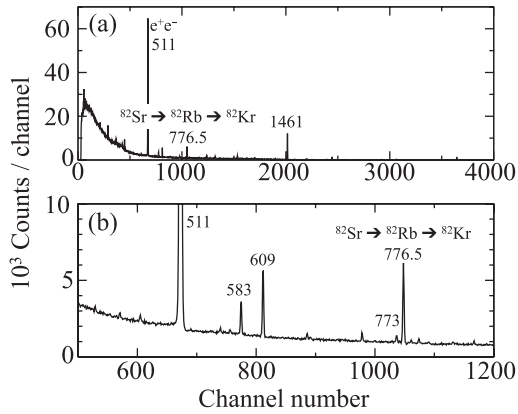

FIG. 9. (a) Spectrum of rays taken from four samples surrounded by an annihilator. (b) The same spectrum showing only the region near the 776.5 keV transition, which is isolated and resolved from the 773 keV γ ray from the background.

(vi) potential clock differences between implantation and γ-measurement data acquisitions, which were assumed to be not more than 5 min, applied on each 30 s time bin.

The largest contributions to the uncertainty in the number of atoms remaining were implantation efficiency (65%) and the data acquisition live time (35%). All others contributed at the 10^{-4} level or less. The implantation efficiency has two values because a magnetic steerer on the beam line failed during the implantation and caused the beam to shift slightly. The time of the failure, determined from the facility logs, occurred during the latter half of sample 2 and all of sample 3. The ring (19–25 mm diameter) of material surrounding sample 3 was measured for 776.5 keV γ rays in an attempt to determine if any ^{82}Sr missed the implantation foil. There was indeed slight activity on the ring, whereas other rings indicated no activity. The relative yield of ring 3 versus sample 3 indicated that 0.5(3)% of the sample's activity was on the ring. Therefore, for sample 3 and the latter half of sample 2, an additional correction was applied. An analysis of the effects of the steerer and the geometry of the experiment indicated that no implants should have occurred outside the ring holding the aluminum foil.

The γ-ray spectrum taken over a 20-day measurement is shown in Fig. 9. The 776.5 keV γ-ray yield was measured to be 13660(160) from a total of $1.895(34) \times 10^8$ decays. The absolute photopeak efficiency for the 776.5 keV γ ray was 0.0004872(58). The data was further corrected by 1.0088(2) for summing with the 511 keV annihilation radiation. Taking these corrections into account, the fractional number of 776.5 keV γ rays emitted per ^{82}Rb decay following the decay of ^{82}Sr is 0.1493(37).

IV. CONCLUSION

The decay of the ^{82}Sr-^{82}Rb generator, used in PET imaging of the heart muscle, was investigated using ion-implantation techniques. A beam of radioactive ^{82}Sr was developed and accelerated above 2.5 MeV per nucleon. This beam was detected by an ionization chamber, and individual ions were identified by their energy loss and implanted in thin foils. Two methods of determining the number of ^{82}Sr atoms implanted were averaged and the subsequent decay of the atoms to ^{82}Rb and ^{82}Kr was measured by a Ge detector. The number of 776.5 keV transitions per decay of ^{82}Rb following the decay of ^{82}Sr was determined to be 0.1493(37), in agreement with the previously accepted value of 0.1508(16).

This technique measures directly the number of atoms in the implanted sample, and hence only the absolute efficiency of the Ge analysis station needs to be calibrated. This technique offers different systematic errors than others that rely on chemical separation coupled with relative measurements. Any isotope with suitable half-life that can be made into a beam and accelerated can be used with this technique.

ACKNOWLEDGMENTS

We thank the HRIBF staff for their help in this research. In particular, the mechanical engineering design of James W. Johnson is gratefully acknowledged. We also thank Ted Barnes, who informed and encouraged us to tackle this problem. This research is sponsored by the Office of Nuclear Physics, US Department of Energy under Contracts No. DE-AC05-00OR22725 (ORNL), No. DE-FG02-96ER40983 (UTK), and No. DE-AC05-06OR23100 (ORAU).

[1] Appl. Radiat. Isot. **38**, 171 (1987), in this issue, edited by S. L. Waters and B. M. Coursey.
[2] S. M. Judge, M. J. Woods, S. L. Walters, and K. R. Butler, Appl. Radiat. Isot. **38**, 185 (1987).
[3] D. D. Hoppes, B. M. Coursey, F. J. Schima, and D. Yang, Appl. Radiat. Isot. **38**, 195 (1987).
[4] H.-W. Muller, Nucl. Data Sheets **50**, 1 (1987).
[5] J. K. Tuli, Nucl. Data Sheets **98**, 209 (2003).
[6] J. A. Winger *et al.*, Phys. Rev. Lett. **102**, 142502 (2009).
[7] S. V. Ilyushkin *et al.*, Phys. Rev. C **80**, 054304 (2009).
[8] J. R. Beene, D. W. Bardayan, A. Galindo-Uribarri, C. J. Gross, K. L. Jones, J. F. Liang, W. Nazarewicz, D. W. Stracener, B. A. Tatum, and R. L. Varner, J. Phys. G **38**, 024002 (2011).
[9] Y. Liu, J. M. Cole, C. A. Reed, C. L. Williams, and G. D. Alton, in *Proc. 17th International Conference on the Applications of Accelerators in Research and Industry*, AIP Conf. Proc. 680 (American Institute of Physics, Woodbury NY, 2003), p. 1017.
[10] D. W. Stracener, G. D. Alton, R. L. Auble, J. R. Beene, P. E. Mueller, and J. C. Bilheux, Nucl. Instrum. Methods Phys. Res. A **521**, 126 (2004).
[11] C. J. Gross *et al.*, Eur. Phys. J. A **25**, 115 (2005).
[12] Sources from Eckert and Ziegler Isotope Products, [www.isotopeproducts.com].
[13] Philip R. Bevington, *Data Reduction and Error Analysis for the Physical Sciences*, (McGraw-Hill, New York, 1969); Excel 2007 Windows Edition, Microsoft Corporation.
[14] S. M. Judge, A. M. Privitera, and M. J. Woods, Appl. Radiat. Isot. **38**, 193 (1987).